Dataset Curation and Deep Learning for Satellite Image Inpainting

Report submitted for completion of training Programme of Space Applications Centre

Submitted by Shikha Sheth (Registration No. RS02086)
B.Tech. (Computer Science and Engineering)

Under the guidance of

Mr. Ashutosh Gupta
SCI/ENG – SF HDPD/ODPG/SIPA
Space Applications Centre, (ISRO) Ahmedabad

Institution CHARUSAT University,
Changa, Gujarat – 382115

SRTD-RTCG-MISA
Space **A**pplications **C**entre (ISRO)
Ahmedabad, Gujarat
16 December 2024 to 09 April 2025

CERTIFICATE

This is to certify that the report entitled “Dataset Curation and Deep Learning for Satellite Image Inpainting” submitted by Shikha Sheth, is a record of bona fide work carried out by her under my supervision during the period, 16. 12. 2024 to 09. 04. 2025. The contents of this report have not been submitted and will not be submitted either in part or in full, for the award of any other degree or diploma in this institute or any other institute or university.

Mr. Ashutosh Gupta SCI/ENG – SF

SAC – Space Applications Centre

High Resolution Data Processing Division (HDPD)

Optical Data Processing Group (ODPG)

Signal and Image Processing Area (SIPA)

ACKNOWLEDGEMENT

I express my sincere gratitude to **Mr. Devakanth Naidu**, Head, SIPA-ODPG-HDPD. for providing me the opportunity to work on this project at the Space Application Centre, ISRO. I would also like to sincerely thank my guide **Mr. Ashutosh Gupta** for sharing his valuable insights and constantly assisting in all possible ways throughout this internship. Finally, I would like to thank the entire team of SIPA/ODPD/HDPD and SIPA/PMPG/PSPD for their constant support. Lastly, I would like to thank **Dr. S P Vyas,** Head, Scientific Research and Training Division (SRTD) for giving me this opportunity to work in SAC, ISRO, Ahmedabad.

Thanks,
Shikha Sheth

ABSTRACT

Remote sensing satellites like Landsat-7 provide valuable Earth observation data, but sensor failures, such as the Scan Line Corrector (SLC)-off issue, have led to missing or corrupted pixel regions in images. This research focuses on generating a comprehensive dataset and applying deep learning-based image inpainting techniques to restore missing data in Landsat-7 images.

A paired dataset was systematically constructed using Landsat-7 (corrupted and uncorrupted) and Landsat-8/9 as reference images. The dataset consists of cropped 256×256 image chips, organized across multiple environmental conditions including water bodies, mountainous terrain, snow-covered areas, urban regions, and forest landscapes. Synthetically corrupted versions of valid Landsat-7 images were generated using a structured masking approach, ensuring realistic degradation patterns.

The curated dataset was validated by applying the LaMa (Large-Mask) image inpainting model. This demonstrates the dataset's readiness for satellite image restoration tasks and provides a benchmark for future model development.

TABLE OF CONTENTS

LIST OF FIGURES

LIST OF TABLES

Abbreviations

- ETM+ – Enhanced Thematic Mapper Plus
- OLI – Operational Land Imager
- TIRS – Thermal Infrared Sensor
- SWIR – Short Wave Infrared
- NCC – Normalised Cross Correlation
- LaMa – Large Mask Inpainting Model

CHAPTER 1: INTRODUCTION

1.1 PROBLEM STATEMENT

The presence of missing data in Landsat-7 imagery due to the SLC-off issue presents a major challenge for remote sensing applications. Traditional interpolation or gap-filling methods often fail to preserve spatial and spectral consistency, especially in regions with complex land cover patterns. There is a pressing need to develop a clean, standardized, and realistic dataset that can be used to evaluate and apply modern image inpainting techniques for satel- lite image restoration.

Moreover, deep learning-based inpainting models have shown promising results in natural image restoration, but their applicability to satellite imagery, especially with large missing regions, remains under-explored due to the lack of publicly available benchmark datasets.

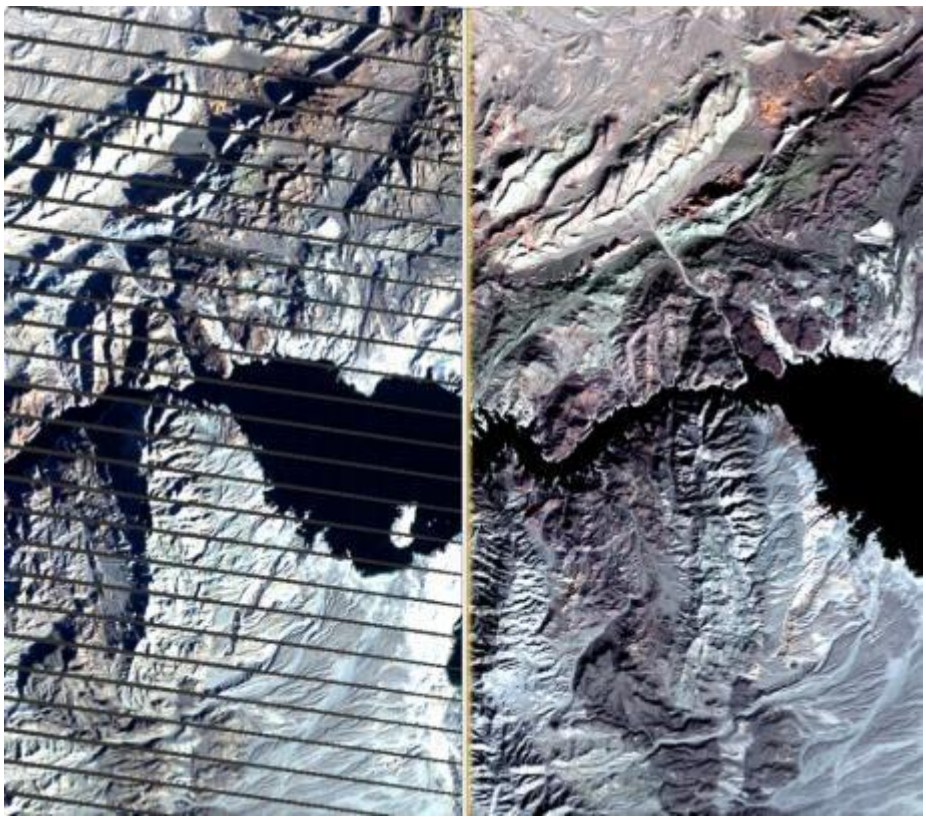

Figure 1 SLC failure comparison

1.2 PURPOSE

The primary purpose of this study is to address the data loss issue in **Landsat-7 imagery** caused by the **Scan Line Corrector (SLC)-off failure**, which results in missing pixel regions across vast areas of satellite scenes. Given the significance of Landsat-7 data in long-term Earth observation, restoring these images is critical for environmental monitoring, change detection, and scientific research.

The study focuses on two integral aspects:

- Generation of a structured and high-quality paired dataset tailored for satellite image inpainting tasks, covering various land surface types.
- Application of a deep learning-based inpainting method, LaMa (Large Mask Inpainting) model, designed to handle large-area corruptions with high- resolution detail using Fourier convolutions.

Together, these elements aim to facilitate reliable restoration of missing data in remote sensing imagery, improving data usability and supporting downstream applications.

1.3 OBJECTIVE

A key objective of this work is the construction of a large-scale, paired, and systematically organized dataset that supports the training and evaluation of image inpainting models. The dataset comprises 256×256 image chips created from Landsat-7 and corresponding Landsat-8/9 images, covering varied environmental features such as water bodies, forests, snow-covered areas, mountains, and urban regions. Valid Landsat-7 images were synthetically corrupted using structured masks that realistically emulate SLC-off degradation patterns. This dataset serves as a critical foundation for benchmarking restoration models and is a major contribution of the work. The deep learning model selected for this task is LaMa (Large Mask Inpainting), a resolution-robust architecture based on Fast Fourier Convolutions as introduced by Suvorov et al. in their work *"Resolution-Robust Large Mask Inpainting with Fourier Convolutions"*.

1.4 SCOPE

The scope of this research extends across two major fronts: dataset generation and inpainting model application. On the dataset front, it includes automated extraction, preprocessing, and corruption of multispectral satellite data from multiple Landsat missions. On the modeling front, it involves the adaptation and evaluation of the LaMa architecture to the remote sensing domain, particularly for handling large and irregular missing regions. The outcomes of this work contribute to both the scientific community and practical applications, enabling enhanced restoration of satellite archives for climate research, land use monitoring, and environmental change detection.

CHAPTER 2: DATASET

2.1 DATASET COLLECTION

The dataset used in this study was constructed using imagery from the Landsat program, specifically from Landsat-7 (ETM+ sensor) and Landsat-8/9 (OLI/TIRS sensor), made available through the USGS Earth Explorer. Landsat-7 has been affected by a known sensor issue—the Scan Line Corrector (SLC)-off malfunction—which introduced systematic gaps in the acquired images post- May 2003. In contrast, Landsat-8/9 provides continuous, high-quality multispectral observations, making it suitable as a reference for restoration tasks.

To support robust deep learning-based image inpainting, a comprehensive dataset of spatially and temporally aligned image chips was generated. The dataset was built by selecting approximately 80 representative Landsat scene locations from the USGS Earth Explorer, with each scene covering an area of 185 km × 180 km at 30- meter resolution. Selection focused on geographic and environmental diversity, including snow-covered zones, mountain ranges, forests, water bodies, and urban regions.

For each selected scene, both Landsat-7 and corresponding Landsat-8 or Landsat-9 images were downloaded and processed. Scenes were chosen to ensure the Landsat- 7 image exhibited SLC-off gaps, while the corresponding Landsat-8/9 image— acquired within a short temporal window—served as a reference for uncorrupted observation of the same area. Using spatial metadata and coordinate alignment, each scene was co-registered and cropped to extract multiple 256 × 256-pixel chips. These chips are stored as 16-bit multi-band arrays in .npy format and as PNG images for visual inspection. Landsat-7 chips use bands 3-2-1 for RGB rendering, while Landsat-8/9 uses bands 4-3-2.

Each valid Landsat-7 chip was further processed to generate three synthetically corrupted variants. A structured masking approach was employed using a real SLC- off region sampled from the first partially corrupted chip of each scene. This mask, capturing the authentic degradation pattern, was reused to corrupt valid Landsat-7 chips consistently. The resulting corrupted chips retain the original pixel values outside the masked regions, while the missing regions are replaced with zeros or

NaNs, replicating the scan-line loss. This results in a total of four variants per original chip: one valid, three corrupted, and one corresponding reference from Landsat-8/9.

The data is systematically organized into a hierarchical directory structure by scene ID, with subfolders for Landsat-7, synthetically corrupted Landsat-7, and reference Landsat-8/9. Each subfolder contains both .npy arrays and .png RGB visualizations. The final dataset comprises over 40,000 multispectral chips, forming a large, diverse benchmark for training and evaluating deep learning-based image inpainting models on satellite data.

This curated dataset plays a central role in this research and contributes significantly to the remote sensing community by addressing the scarcity of publicly available, high-quality datasets for SLC-off image restoration tasks.

CHAPTER 3: DATA PREPERATION AND ANALYSIS

3.1 DATASET STRUCTURE AND COMPOSITION

The dataset developed for this study focuses on addressing missing data in Landsat- 7 imagery caused by the Scan Line Corrector (SLC)-off failure. It comprises image triplets:

- Valid, uncorrupted Landsat-7 image chips,
- Their synthetically corrupted counterparts mimicking SLC-off artifacts, and
- Aligned reference chips from Landsat-8/9.

Each image chip is of size 256×256 pixels and represents a spatially matched patch across sensors and corruption states. These chips are drawn from 80 distinct Landsat scenes distributed across a variety of terrain types.

Each folder contains RGB PNGs and full-band NPY arrays. PNGs are generated using bands 3-2-1 for Landsat-7 and 4-3-2 for Landsat-8/9, while NPY files store all spectral bands (6 for Landsat-7 and 7 for Landsat-8/9) as 3D arrays.

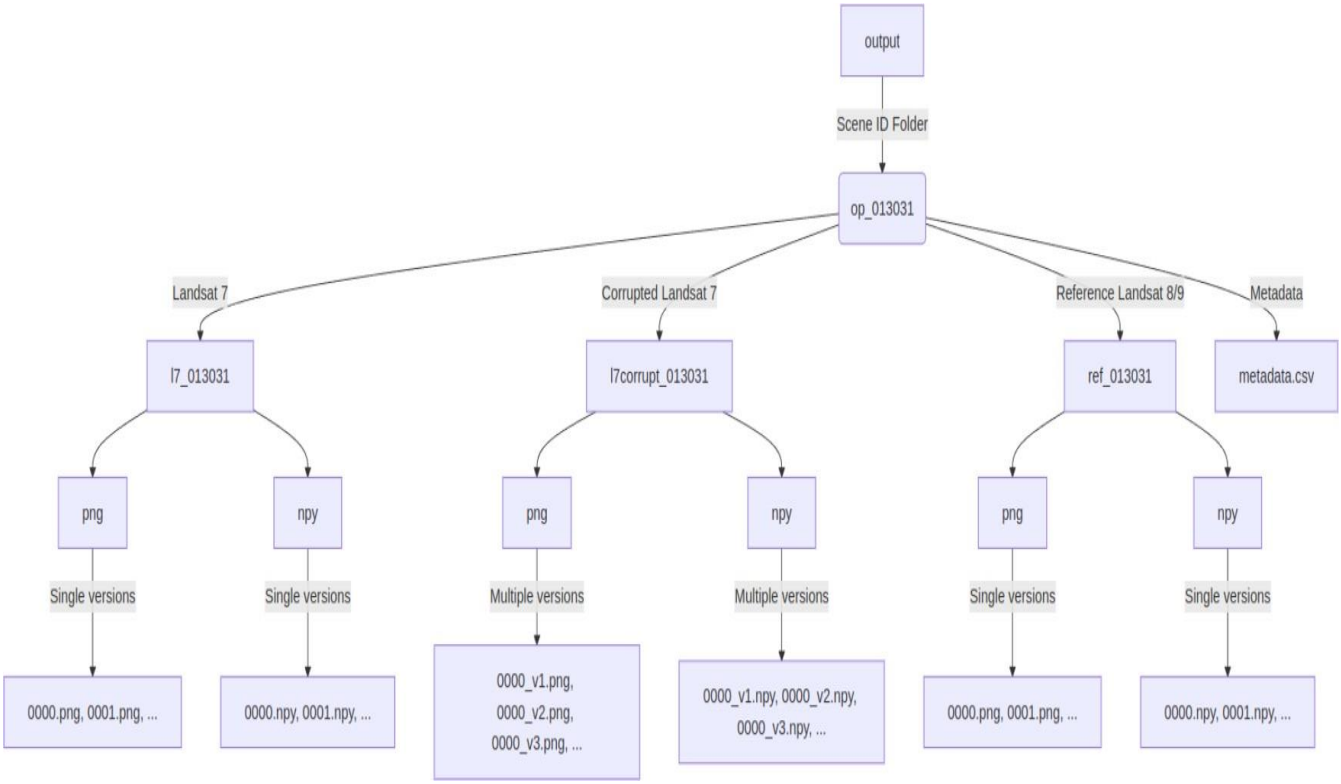

Figure 2 Dataset Structure

3.2 ENVIRONMENTAL DIVERSITY AND SCENE SELECTION

To ensure the robustness and generalization of inpainting models, data was sourced from scenes representing five major environmental types:

- Water bodies
- Mountains
- Snow-covered terrain
- Urban settlements
- Forested regions

This diversity enables the model to learn context-aware restoration strategies suitable across varying reflectance patterns, shadows, textures, and spectral responses.

3.3 SYNTHETIC CORRUPTION

One of the most crucial aspects of this dataset is the creation of realistically corrupted Landsat-7 images.Instead of random masking, synthetic corruption is generated using real SLC-off masks extracted from partially valid scenes. These masks reflect true geometric line-drop patterns. Each valid image is masked using three different SLC- off masks, generating three distinct corrupted versions.

This structured corruption strategy ensures that the model is trained to inpaint images that simulate real-world artifacts in a controlled, repeatable way, maintaining scientific relevance while augmenting the dataset volume.

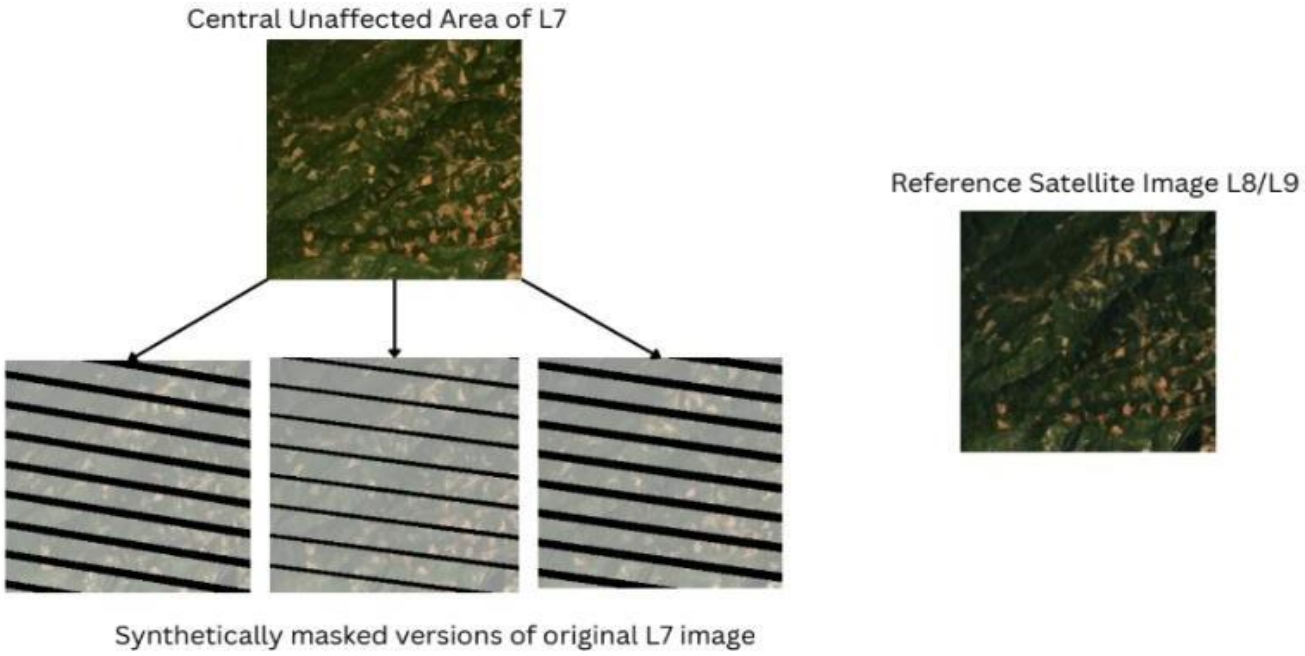

Figure 3 Curated Data Format

3.4 LaMa ADAPTATION

LaMa (Large-Mask Inpainting), is designed to handle high-resolution images with large missing regions. LaMa employs Fast Fourier Convolutions (FFC) to capture both global and local context, making it highly suitable for inpainting the long, structured gaps caused by the SLC-off failure in Landsat-7 imagery.

To utilize this model effectively, the custom dataset was adapted to meet LaMa's architectural requirements:

- Input Format: Each input sample includes a 256×256 Landsat-7 chip with synthetic SLC-off-like corruption, alongside a corresponding binary mask denoting the corrupted regions.
- Output Supervision: The original, uncorrupted Landsat-7 chip serves as the ground truth for supervision.
- Data Channels: For inpainting, the RGB versions (bands 3, 2, 1) of the multispectral data were used to generate 3-channel PNG images. Binary masks were also saved as PNGs.

The LaMa model was provided with data in the following format:

- Original (ground truth) images
- Corrupted images and corresponding binary masks
- LaMa model predictions after inpainting

This adaptation enables the LaMa architecture to focus on learning to reconstruct structured missing patterns under a supervised setting, using realistic satellite data. The ability of LaMa

to handle large-scale contextual reconstruction directly aligns with the nature of SLC-off defects.

3.5 DATA VARIETY AND CORRELATION ANALYSIS

The constructed dataset comprises a wide range of land cover types, including forested regions, mountainous terrain, snow-dominated zones, urban settlements, and water bodies. These samples were selected from geographically dispersed locations to ensure that the dataset encapsulates diverse environmental and spectral characteristics. The inclusion of this spatial and thematic variety is essential for evaluating inpainting models under varying input conditions, thereby strengthening the dataset's utility and relevance.

To quantitatively assess the spectral similarity between temporally aligned image chips from different satellite sources, Normalized Cross-Correlation (NCC) was employed. For each selected scene, corresponding 256×256 image chips from Landsat 7 and Landsat 8/9 were analyzed band-wise. The NCC values were calculated to measure how closely the two satellite images correspond at a pixel level, reflecting inter-sensor consistency in surface reflectance across various terrains.

The resulting correlation distributions reveal patterns of agreement across multiple land types, demonstrating the capability of the dataset to serve as a benchmark for image restoration tasks. Additionally, graphical summaries of the correlation values and the geographical spread of the selected chips further illustrate the dataset's coverage and the robustness of chip alignment between the satellite sources. This comprehensive analysis confirms the dataset's strength in capturing real-world variability while maintaining meaningful spectral correspondence.

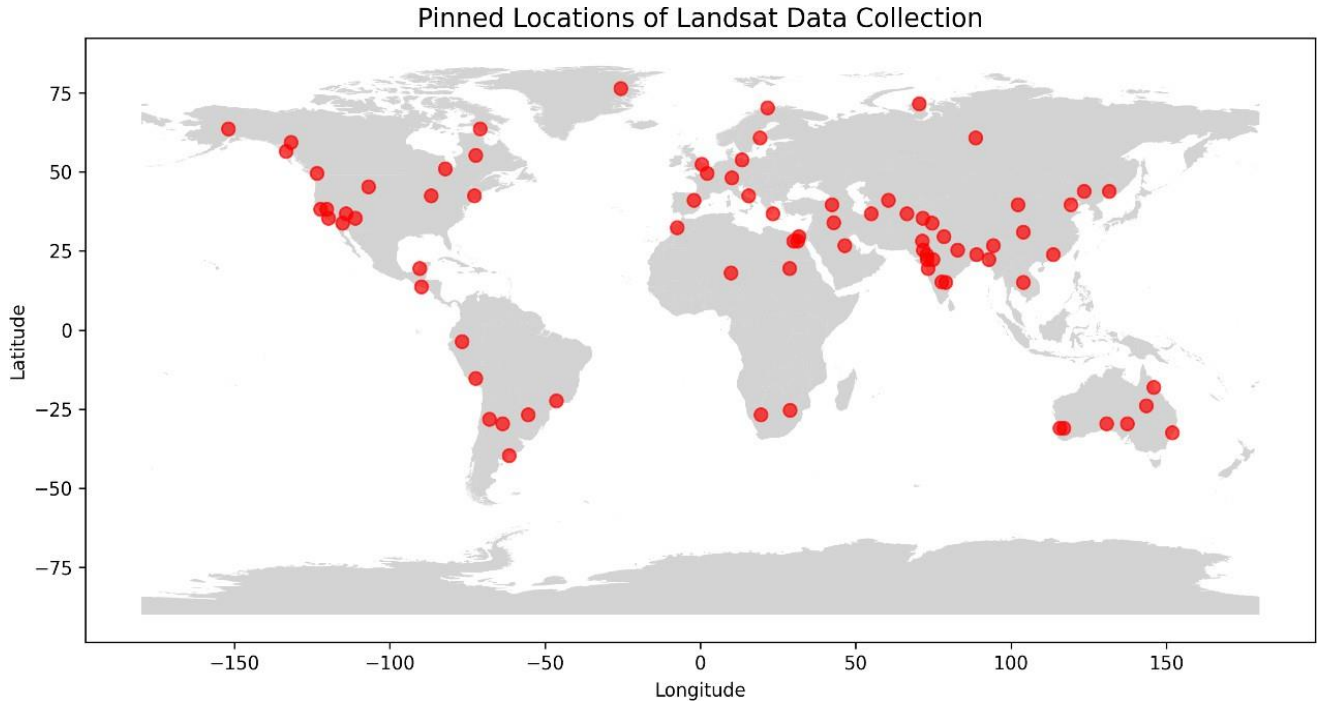

Figure 4 Locations of collected scenes across the world

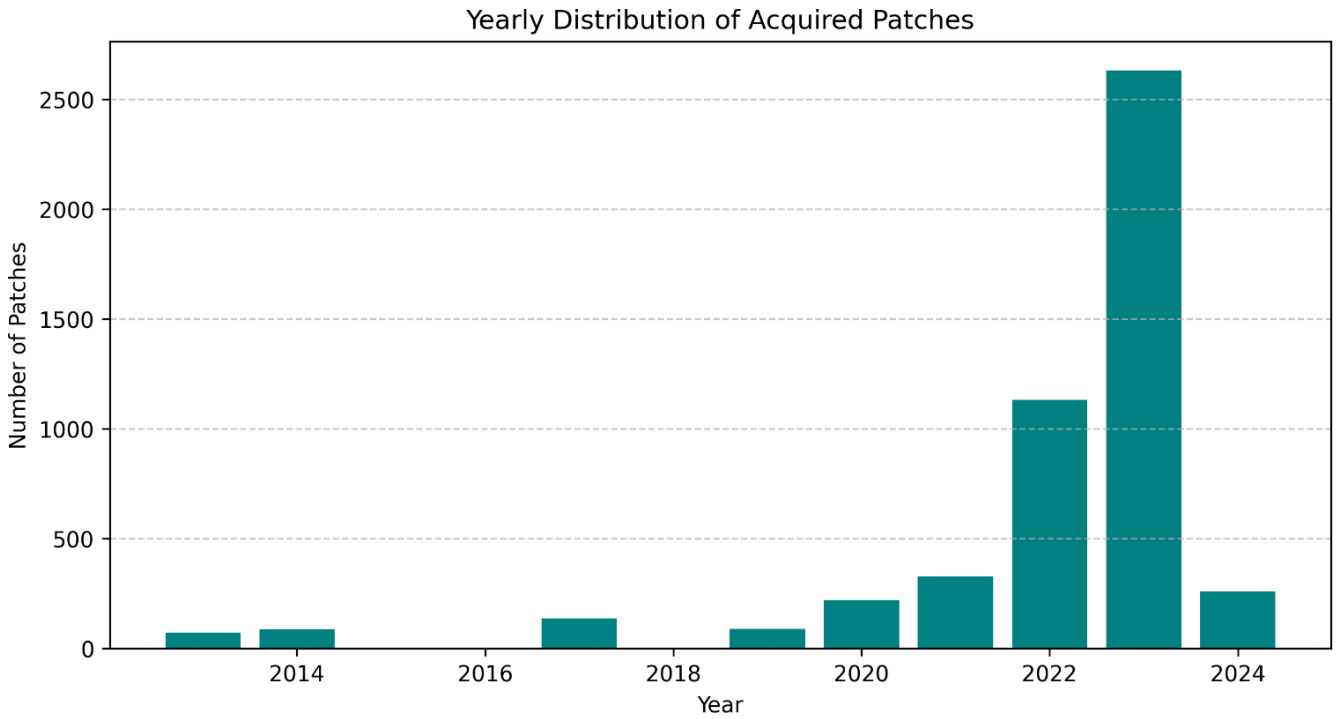

Figure 5 Yearly distribution of scenes

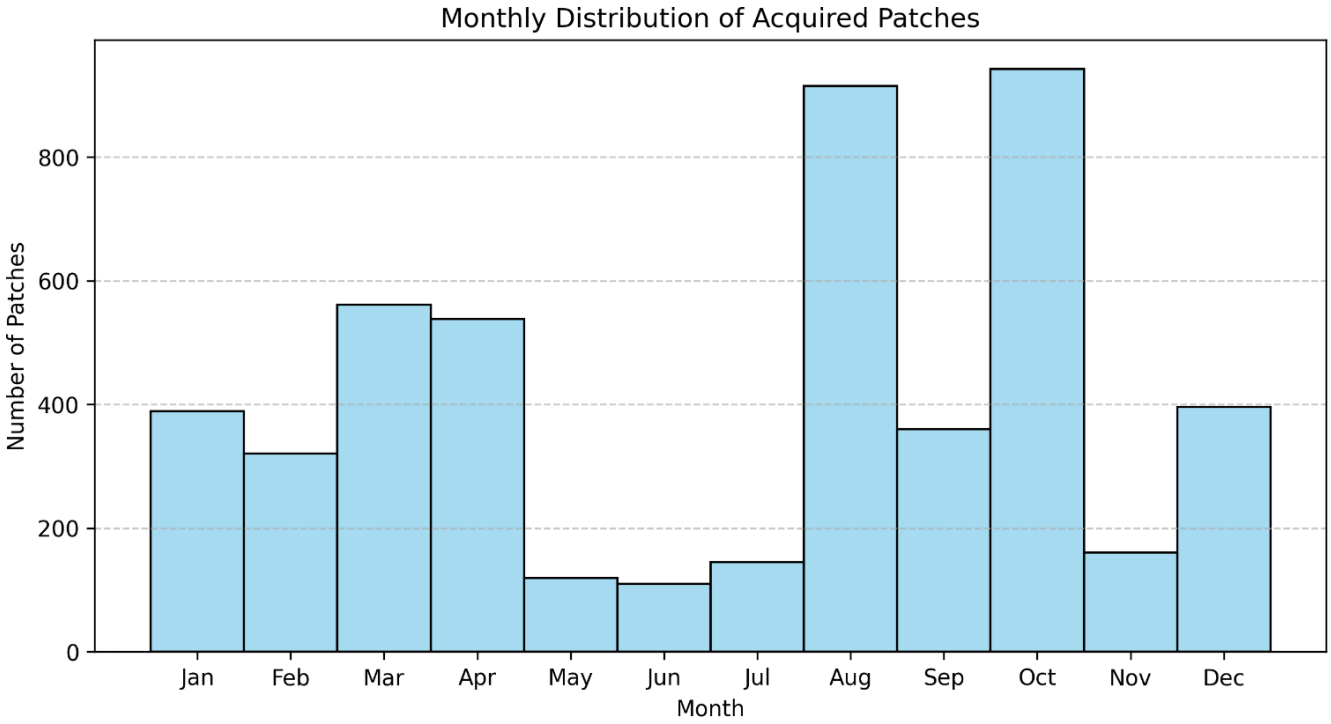

Figure 6 Monthly distribution of scenes

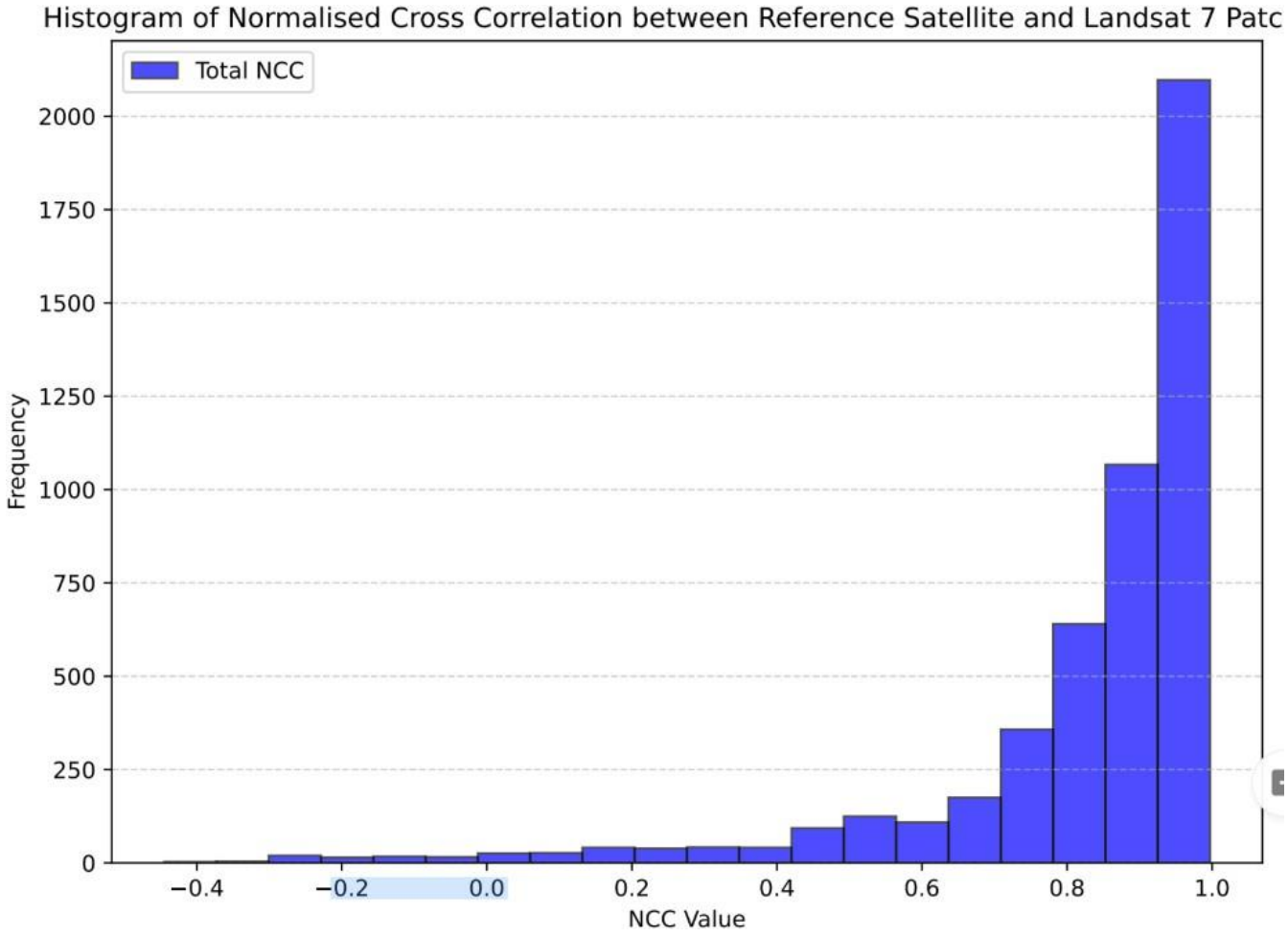

Figure 7 NCC Correlation of patches

CHAPTER 4: BAND COMPARISON ACROSS SATELLITES

4.1 SPECTRAL BAND COMPARISON ACROSS SATELLITES

In Restoration of multispectral satellite imagery requires careful consideration of the spectral and spatial properties of the input data. Satellite platforms such as Landsat-7 and Landsat-8/9 provide imagery captured using sensors with distinct band configurations, central wavelengths, and resolutions. These differences influence the compatibility of datasets used for training, evaluation, and restoration tasks.

Ensuring spectral alignment between corrupted images and reference counterparts is essential for effective dataset generation and inpainting performance. Variations in shortwave infrared, near-infrared, and visible bands must be accounted for to preserve radiometric consistency across platforms. Comparative analysis of these bands aids in selecting corresponding channels during preprocessing and in guiding architectural decisions when developing deep learning models for image restoration.

BANDS	LANDSAT7	LANDSAT8	LANDSAT9	SENTINEL2
1	-	Coastal Aerosol (0.43 - 0.45 µm) 30 m	Visible Coastal Aerosol (0.43 - 0.45 µm) 30-m	Coastal Aerosol (0.433 – 0.45 µm) 60m
2	Blue (0.45 – 0.515 µm) 30 m	Blue (0.450 - 0.51 µm) 30 m	Visible Blue (0.450 - 0.51 µm) 30-m	Blue (0.458– 0.523) 10m
3	Green (0.525 – 0.605 µm) 30 m	Green (0.53 - 0.59 µm) 30 m	Visible Green (0.53 - 0.59 µm) 30-m	Green (0.543 – 0.578 µm) 10-m
4	Red (0.63 – 0.69 µm) 30 m	Red (0.64 - 0.67 µm) 30 m	Red (0.64 - 0.67 µm) 30-m	Visible Red (0.650– 0.680 µm) 10-m
5	-	-	-	Red Edge 1 (0.698 – 0.713 µm) 20-m
6	-	-	-	Red Edge 2 (0.733 – 0.748 µm) 20-m
7	-	-	-	Red Edge 3 (0.773 – 0.793 µm) 20-m

8	Near Infrared (NIR) (0.76 – 0.90 µm) 30 m	Near-Infrared (0.85 - 0.88 µm) 30 m	Near-Infrared (0.85 - 0.88 µm) 30-m	NIR (Near Infrared) (0.785 – 0.899 µm) 10-m
9	-	-	-	Narrow NIR (Red Edge) (0.855 – 0.875 µm) 20-m
10	Shortwave Infrared (SWIR) (1.55 – 1.75 µm) 30 m	SWIR 1(1.57 - 1.65 µm) 30 m	SWIR 1(1.57 - 1.65 µm) 30-m	SWIR 1 (Shortwave Infrared 1) (1.565 – 1.655 µm) 20-m
11	Mid Infrared (2.08 – 2.35 µm) 30 m	SWIR 2 (2.11 - 2.29 µm) 30 m	WIR 2 (2.11 - 2.29 µm) 30-m	SWIR 2 (Shortwave Infrared 2) (2.100 – 2.280 µm) 20-m
12	Panchromatic (PAN) (0.52 - 0.90 µm) 15 m	Panchromatic (PAN) (0.50 - 0.68 µm) 15 m	Panchromatic (PAN) (0.50 - 0.68 µm) 15-m	-
13	-	-	-	Water Vapour (0.935 – 0.955 µm) 60-m
14	-	Cirrus (1.36 - 1.38 µm) 30 m	Cirrus (1.36 - 1.38 µm) 30-m	Cirrus (1.360 – 1.390 µm) 60-m
15	Thermal Infrared (TIR) (10.40 – 12.50 µm) 60m Low Gain/High Gain	TIRS 1 (10.6 - 11.19 µm) 100 m	TIRS 1 (10.6 - 11.19 µm) 100-m	-
16	-	TIRS 2 (11.5-12.51 µm) 100 m	TIRS 2 (11.5-12.51 µm) 100-m	-

Table 1 Band Comparison

CHAPTER 5: MODEL ARCHITECTURE AND RESULT

5.1 LaMa ARCHITECTURE

The LaMa (Large Mask Inpainting) model, introduced by Suvorov et al. in the paper *"Resolving Issues with Deep Image Inpainting"*, presents a novel approach to image inpainting, specifically designed to handle large missing regions with high resolution and semantic consistency. Unlike traditional convolutional neural network architectures, LaMa leverages Fast Fourier Convolutions (FFCs) to extend the receptive field efficiently, allowing the model to capture long-range spatial dependencies without sacrificing computational efficiency.

The architecture of LaMa is fundamentally encoder-decoder based, but with a significant distinction—standard convolutions are replaced with a hybrid of global (Fourier-based) and local convolutions in the later encoder layers. This combination allows the model to maintain fine-grained details while understanding broader contextual cues from the entire image. Additionally, the architecture incorporates gated convolutions and perceptual losses, which enhance the model's ability to generate visually plausible and context- aware content in masked regions.

LaMa is also designed to be resolution-robust, which makes it especially suitable for high-resolution satellite image inpainting tasks. Its training scheme includes high- frequency reconstruction loss and adversarial learning to further refine the realism and texture of inpainted areas. The model outperforms conventional approaches in both qualitative and quantitative metrics, particularly in scenarios involving irregular or large missing regions.

In this work, the LaMa model is applied to restore missing data in Landsat-7 imagery caused by the Scan Line Corrector (SLC)-off failure. Its ability to handle large corrupted regions with contextual and spectral consistency makes it a compelling solution for remote sensing image restoration. The model's robustness and architectural innovations contribute significantly to the effectiveness of deep learning-based inpainting for Earth observation datasets.

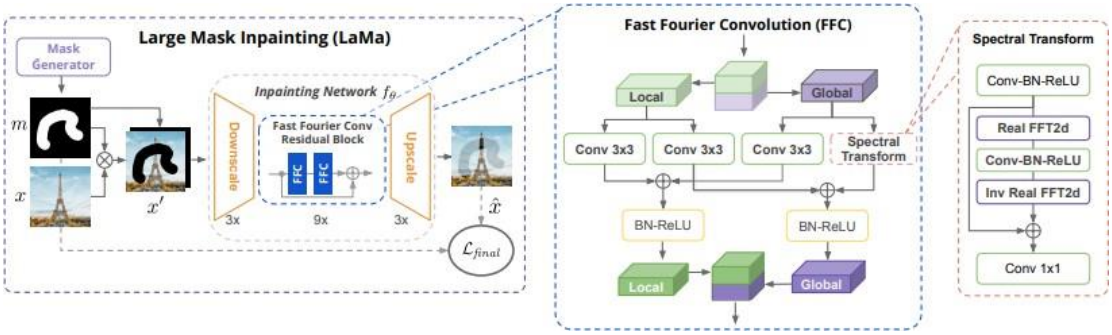

Figure 8 LaMa Architecture

5.2 MODEL RESULT

This chapter presents the quantitative evaluation of the inpainting performance using the LaMa Inpainting model on a selected subset of the prepared dataset. The evaluation was carried out on 10 representative image chips that include synthetically corrupted Landsat 7 scenes and their corresponding ground truth (original) versions. Two standard image quality metrics were used to assess the reconstruction quality: Peak Signal-to-Noise Ratio (PSNR) and Structural Similarity Index Measure (SSIM).

The following results summarize the comparative analysis between:

- **Corrupted vs. Original** (to quantify degradation)
- **Inpainted vs. Original** (to measure restoration)

Evaluation Pair	Average PSNR	Average SSIM
Corrupted vs. Original	17.93	0.6608
Inpainted vs. Original	32.16	0.8993

The PSNR for the corrupted images was recorded at 17.93 dB, indicating a moderate level of degradation due to the applied synthetic masking. After restoration using the LaMa inpainting model, the PSNR improved significantly to 32.16 dB, reflecting a substantial enhancement in pixel-level fidelity and signal reconstruction.

Similarly, the SSIM values showed a marked increase from 0.6608 to 0.8993, suggesting that the structural integrity and spatial details of the images were effectively recovered. The high SSIM further confirms the model's ability to preserve perceptual and contextual similarity with the original data.

These improved results highlight the potential of deep learning-based inpainting for accurate restoration of masked satellite imagery. While promising, further validation on a larger and

more diverse dataset would strengthen these findings.

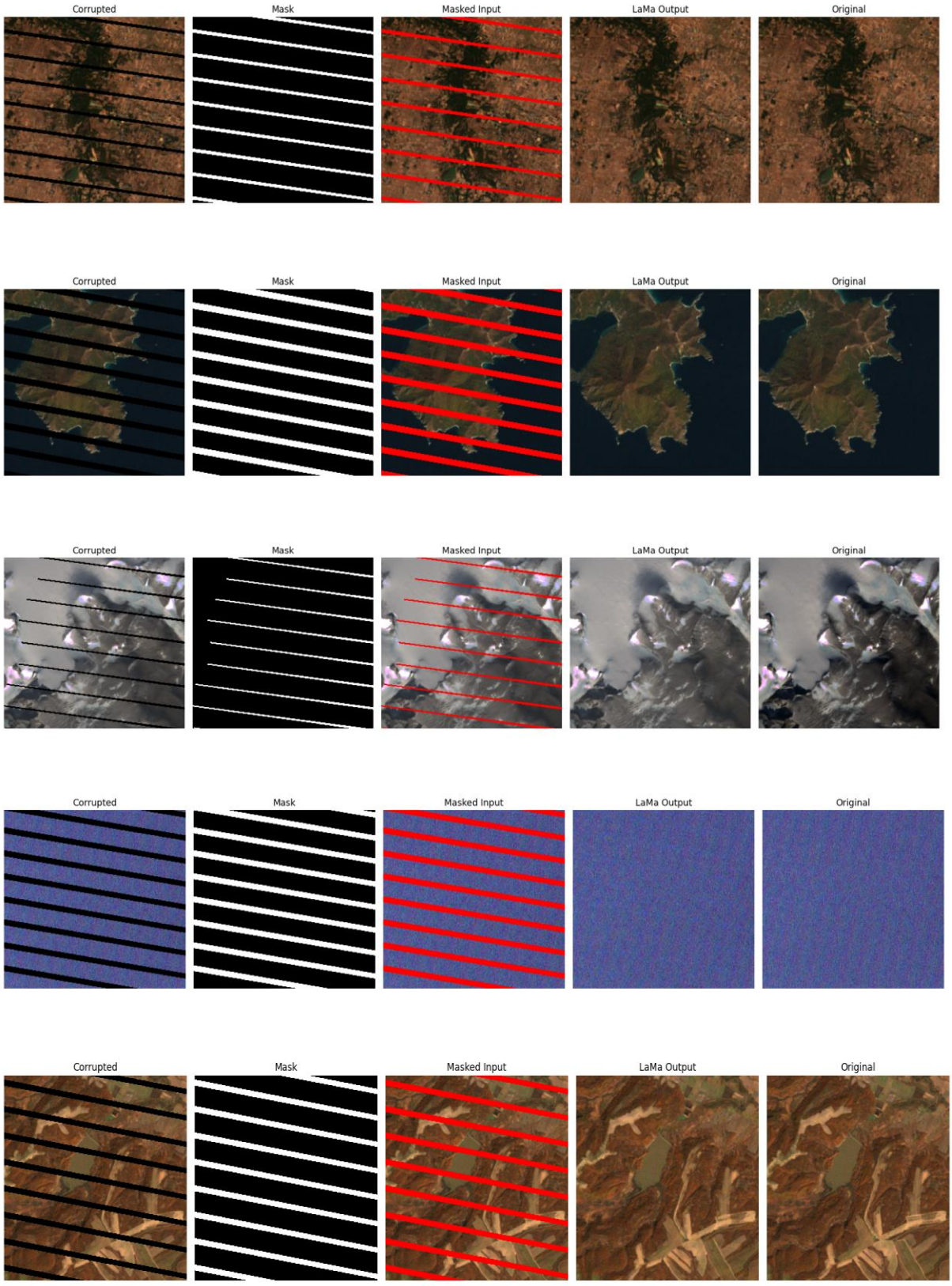

Figure 9 Inpainted Result

5.3 EXPLORATION OF ADDITIONAL INPAINTING TECHNIQUES

In addition to the LaMa inpainting model, several advanced deep learning techniques were investigated to enhance the restoration quality of masked satellite imagery. These included Deep Image Prior (DIP), Convolutional Conditional Neural Processes (ConvCNP), and a diffusion-based inpainting model. Despite their theoretical potential, these approaches could not be successfully implemented within the project timeline. The DIP and ConvCNP models posed significant challenges in adapting to the specific requirements of satellite data, demanding substantial architectural adjustments and hyperparameter tuning. The diffusion-based model, though promising in natural image domains, resulted in perceptually inconsistent and hallucinated outputs when applied to multispectral satellite images. The corresponding codebases explored during this phase are:

- **Deep Image Prior**: https://github.com/petrovskaia/deep-image-prior-landsat
- **ConvCNP**: https://github.com/YannDubs/Neural-Process-Family/tree/master
- **Diffusion-Based Inpainting**: https://github.com/SatelliteShorelines/SatelliteInPaint

These exploratory efforts, while not yielding deployable results, provided insights into the challenges of applying general-purpose deep learning models to satellite image inpainting tasks.

CHAPTER 6: CONCLUSION

This study focused on the restoration of Landsat 7 SLC-off imagery using deep learning- based image inpainting. A comprehensive dataset was constructed by aligning and extracting paired chips from Landsat 7 and Landsat 8/9 imagery across diverse terrain types. Synthetic corruption masks were applied to emulate real-world scan-line failures, allowing controlled evaluation of restoration algorithms.

The LaMa (Large-Mask) model, which incorporates fast Fourier convolutions for effective inpainting, was applied to a subset of the dataset. Quantitative results based on PSNR and SSIM indicate that LaMa achieved moderate improvements in restoration, with greater structural recovery compared to pixel-level reconstruction. Ice-covered regions demonstrated better restoration quality, while water bodies exhibited weaker performance.

The results demonstrate the viability of deep learning-based approaches for enhancing the utility of Landsat 7 SLC-off data, particularly in certain surface types. The methodology also establishes a reproducible pipeline for future research in satellite image restoration.

CHAPTER 7: LIMITATIONS

While this study successfully demonstrates the feasibility of using deep learning-based inpainting techniques for restoring missing data in Landsat-7 imagery, certain limitations were encountered. The evaluation was conducted on a limited set of 10 image chips, which may not comprehensively represent the diverse environmental and geographical conditions present across the entire dataset. As a result, the findings may not fully capture the generalizability of the model's performance. Additionally, it was observed that the inpainting output varied significantly across different land cover types. The restoration quality was notably better for ice-covered regions, while the model performed comparatively poorly in the case of water bodies, likely due to their textureless and homogeneous appearance. Another important limitation arises from the nature of the corruption used for training and evaluation. Although the masking approach was derived from actual SLC-off patterns, the synthetic corruption may not perfectly mimic the irregularities and complex degradation present in real-world failures, potentially limiting the robustness of the model in practical scenarios.

CHAPTER 8: FUTURE SCOPE

- Integration of Auxiliary Geospatial Data: Incorporating additional spatial information such as NDVI, elevation maps, temporal sequences, or land cover classifications may provide better contextual cues for inpainting models, thereby improving performance.
- Adoption of More Robust Deep Learning Techniques: Future research can explore advanced inpainting frameworks such as attention-based transformer architectures, diffusion models, or hybrid approaches combining convolutional and Fourier techniques. These models are well-suited to handle large missing regions with higher fidelity.
- Multi-Sensor Generalization: The proposed pipeline can be extended to other Earth observation platforms beyond Landsat, such as Sentinel-2 or commercial satellites, allowing cross-sensor restoration and wider applicability.
- Future Publication of Dataset: The dataset generated as part of this work— comprising aligned, masked, corrupted, and reference satellite image chips—is intended to be published in a publicly accessible repository. This will serve as a valuable resource for the remote sensing and deep learning communities to benchmark and develop restoration algorithms on structured SLC-off simulation data.

CHAPTER 9: BIBLIOGRAPY

1. Roman Suvorov, Elizaveta Logacheva, Anton Mashikhin, Anastasia Remizova, Arsenii Ashukha, Aleksei Silvestrov, Naejin Kong, Harshith Goka, Kiwoong Park, Victor Lempitsky. https://arxiv.org/abs/2109.07161

2. Jonathan Gordon, Wessel P. Bruinsma, Andrew Y. K. Foong, James Requeima, Yann Dubois, Richard E. Turner https://arxiv.org/abs/1910.13556

3. Anna Petrovskaia, Raghavendra B. Jana, Ivan V. Oseledets https://arxiv.org/abs/2004.04209

4. James Storey, Pasquale Scaramuzza, Gail Schmidt, Julia Barsi, doi:10.1016/j.cageo.2019.104339.